Non-isothermal Characterization of the Precipitation Hardening of a Cu-11Ni-19Zn-1Sn Alloy

E. DONOSO, M.J. DIÁNEZ, J.M. CRIADO, R. ESPINOZA, and E. MOSQUERA

The precipitation hardening of a Cu-11Ni-19Zn-1Sn alloy has been studied by means of Differential Scanning Calorimetry (DSC), High-Resolution Transmission Electron Microscopy (HRTEM), and hardness measurements. The calorimetric curves, in the range of temperatures analyzed, show the presence of one exothermic reaction followed by an endothermic one. The exothermic DSC peak is due to the segregation of Cu_2NiZn precipitates and it is associated to a noticeable improvement of the mechanical properties of the alloy. The endothermic effect is associated to the dissolution of the Cu_2NiZn precipitates into the copper matrix for restoring the starting Cu-11Ni-19Zn-1Sn homogeneous solid solution. The reaction mechanisms of these processes have been proposed from the kinetic analysis of the exothermic and endothermic DSC signals. The results obtained point out that tin plays a decisive role on the precipitation hardening of the alloy, because age hardening is not observed in the case of a Cu-Ni-Zn ternary alloy of similar composition.

DOI: 10.1007/s11661-017-4063-4

I. INTRODUCTION

THE industry is requiring materials microstructurally stable with a high electrical and/or thermal conductivity and a large corrosion resistance for manufacturing a large number of devices such as welding electrodes, high-performance switches, rocket nozzles, *etc*. Copper is the most promising material for these applications because of its high thermal and electrical conductivity, although a considerable improvement of both mechanical properties and the corrosion resistance would be required for accomplishing the above requirements.[1,2] It has been shown in the literature[3–5] that Cu-Ni-Zn alloys with zinc weight percentages lower than 35 pct, which form homogeneous solid solution with α-Cu structure, are very good candidates for achieving the above purposes because of their high wear and corrosion resistance. On the other hand, Zhou *et al*.[6,7] have recently reported that the addition of a small percentage of aluminum dramatically improves the mechanical properties of the annealed alloy because the addition of this metal promotes the formation of nanosized precipitates of an ordered Cu_2NiZn phase. It is noteworthy to point out that the precipitation hardening improves the electrical and mechanical properties of the alloys, while the cold rolling strengthening leads to a depletion of the electrical conductivity,[6] which explain the large number of papers[8–13] concerning with the strengthening of alloys by precipitation hardening. A better insight in the precipitation hardening mechanism of Cu-Ni-Zn-Al alloys has been very recently achieved[14] from combined analysis of the annealing process by means of High-Resolution Electron Microscopy Transmission (HRTEM), microhardness measurements, and Differential Scanning Calorimetry (DSC). It is noteworthy to point out that DSC has been successfully used in the literature[14–23] for discriminating the successive phase transitions taking place as a function of the annealing temperature of alloys.

Studying the influence that the substitution of aluminum for other metals has on the structural changes undergone during the annealing of Cu-Ni-Zn-based quaternary alloys would be of great interest for improving their mechanical properties. The scope of the present work is to study the structural evolution of a Cu-Ni-Zn-Sn alloy as a function of the aging temperature by means of HRTEM, DSC, and microhardness measurements.

II. EXPERIMENTAL

The Cu-Ni-Zn and Cu-Ni-Zn-Sn alloys used in this work were prepared by melting the stoichiometric mixtures of high-purity metals in an induction furnace under argon atmosphere. The ingots obtained in this way were annealed at 1123 K (850 °C) under argon atmosphere for homogenization and then submitted to successive cold rolling and annealing treatments for 1 hour at 1123 K (850 °C) until achieving plates with a

E. DONOSO and R. ESPINOZA are with the Departamento de Ciencia de los Materiales, Facultad de Ciencias Físicas y Matemáticas, Universidad de Chile, Avda. Tupper 2069, Beauchef 851, 8370456 Santiago, Chile. M.J. DIÁNEZ and J.M. CRIADO are with the Instituto de Ciencia de Materiales de Sevilla, Centro Mixto Universidad de Sevilla-C.S.I.C., Américo Vespucio 49, 41092 Sevilla, Spain. Contact e-mail: dianez@icmse.csic.es E.MOSQUERA is with Departamento de Ciencia de los Materiales, Facultad de Ciencias Físicas y Matemáticas, Universidad de Chile, Beauchef 851, 8370456 Santiago, Chile, and also with the Departamento de Física, Universidad del Valle, A.A. 25360, Cali, Colombia.

Manuscript submitted September 26, 2016.
Article published online March 15, 2017

thickness of 3 mm. These plates were finally heated for 24 hours at 1123 K (850 °C) and tempered by water quenching at room temperature for preserving the α-Cu structure of the homogeneous solid solution. The weight percentage composition determined by chemical analysis is Cu-11.3Ni-19.2Zn-1.1Sn (Cu-11Ni-19Zn-1Sn here after). The same sample of Cu-11Ni-20Zn prepared and structurally characterized by us in a previous work[14] has been used as a reference material.

The DSC diagrams were obtained under an argon flow of 100 cc/min with a DSC TA Instruments, model Q 10, using pure electrolytic copper as a reference material.

An FEI Tecnai ST F20 transmission electron microscope that operates at 200 kV has been used for characterizing the microstructure of the Cu-11Ni-19Zn-1Sn sample.

The Vickers hardness was measured at room temperature after annealing the sample at different temperatures and/or times. The measurements of the VH hardness were carried out with a Duramin-1/-2 Struers microhardness durometer tester by applying a load of 1,9 N during 10 seconds on previously polished sample disks. Each microhardness value was calculated as an average of 10 measurements with a standard deviation of approximately 2 pct.

III. RESULTS AND DISCUSSION

Figure 1 shows the DSC diagram obtained at a heating rate of 0.167 K/s (0.167 °C/s) for the Cu-11Ni-19Zn-1Sn alloy. The DSC of the ternary Cu-11Ni-20Zn alloy has been also included in Figure 1 for a comparison in order to test the influence of the addition of a small percentage of tin on the mechanical properties of the Cu-Ni-Zn alloy. It is noteworthy to point out that the same Cu-11Ni-20Zn sample here reported was used by us in a previous paper[14] as a reference in the study of the aging strengthening of a Cu-12Ni-17Zn-1.7Al alloy. It was concluded that the first exothermic peak of the Cu-11Ni-20Zn alloy in Figure 1 was associated to the formation of the Ll_0 phase of Cu_2NiZn from the supersaturated Cu-11Ni-20Zn α phase, while the second exothermic DSC peak was associated to the $Ll_0 \rightarrow Ll_2$ phase transition. The formation of nanocrystals of a Cu_2NiZn phase coherent with the starting α phase and embedded into the alloy matrix was confirmed by HRTEM.[14]

Figure 1 points out that the two exothermic phase transitions of the Cu-11Ni-20Zn alloy, associated to the formation of the Ll_0 and Ll_2 coherent phases, respectively, are not observed in the DSC trace of the Cu-11Ni-19Zn-1Sn alloy. This behavior is quite different to the one previously reported[14] for a quaternary alloy with similar composition, but containing a small amount of aluminum instead of tin. In such a case, the two DSC peaks corresponding to the segregation of an Ll_0 phase coherent with the alloy matrix and the $Ll_0 \rightarrow Ll_2$ phase transition, respectively, were clearly observed besides an additional strong exothermic peak merging at higher temperatures associated to the precipitation of the Ll_2 phase. The hardness measurements previously reported[14] demonstrated that the strengthening of the Cu-12Ni-17Zn-1.7Al alloy was mainly due to the precipitation of the Cu_2NiZn phase. These considerations suggest that the addition of tin instead of aluminum would promote the direct precipitation of Cu_2NiZn phase in a single step associated to the first DSC exothermic peak of the Cu-11Ni-19Zn-1Sn sample reported in Figure 1. This interpretation is supported by the HRTEM picture shown in Figure 2 that was obtained after annealing the sample at a temperature of 525 K (252 °C), which is close to the temperature at which the exothermic peak was over. This figure clearly shows the formation of nanometrics precipitates similar to those reported by Zhou *et al.*[6,7] for a Cu-10Ni-20Zn-1.2Al alloy and Diánez *et al.*[14] for a Cu-12Ni-17Zn-1.7Al alloy. However, it is noteworthy to point out that the temperature of the DSC exothermic effect associated to the precipitation of Cu_2NiZn from Cu-11Ni-19Zn-1Sn here found is around two hundred degrees lower than the one reported for a quaternary alloy with similar composition but containing aluminum instead of tin.[6,7] This behavior explains that the aging hardening temperature of Cu-Ni-Zn alloys is markedly reduced if aluminum is replaced by tin in the composition of the quaternary alloy.

On the other hand, the DSC endothermic peak in Figure 1 could be attributed to the solution of the precipitates into the matrix. The fact that precipitates were not observed in the TEM picture of the sample annealed at 650 K (377 °C) (not shown) (similar to the HRTEM picture of the starting sample) supports this conclusion. These results suggest that the solvus temperature for the formation of a supersaturated solid solution with composition Cu-11Ni-19Zn-1Sn is considerably lower than the one reported[14] for a quaternary alloy of similar composition but with aluminum instead of tin. In fact, the DSC diagram reported for the Cu-12Ni-17Zn-1.7Al alloy indicates that the solution of the precipitates generated by aging does not occur below 900 K (627 °C) that was the maximum temperature allowed by the DSC equipment used.

The values of the Vickers hardness, measured as a function of the time at different annealing temperatures shown in Table I, could allow testing the correlation between the structural changes undergone during the annealing treatment and the strengthening of the alloys. The slight increase of hardness of the Cu-11Ni-20Zn alloy after annealing at 450 K (177 °C), which is in the temperature range of the second exothermic phase transition, shows the poor hardening response of the Ll_2 phase generated at this temperature according with the HRTEM study previously carried out by us on this sample.[14] It must be pointed out that the value of 126 HV obtained for the hardness of Cu-11Ni-19Zn-1Sn-tempered alloy is noticeably higher than the corresponding one to the Cu-Ni-Zn ternary alloy, which demonstrates that the addition of a small amount of tin to this alloy clearly improves its mechanical properties. On the other hand, the results reported in Table I clearly show that the hardness as a function of the time increases by increasing the annealing temperature from 450 K to 525 K (177 °C to

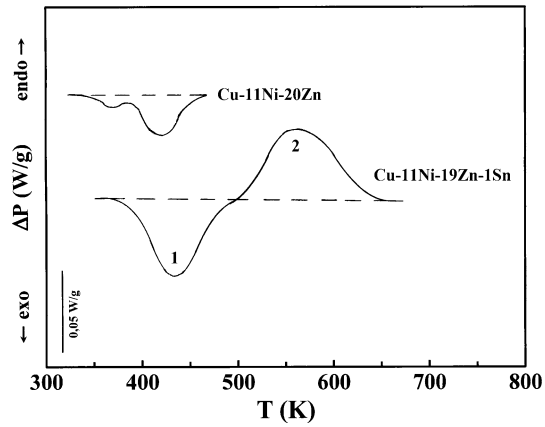

Fig. 1—DSC plots obtained for the Cu-Ni-Zn and Cu-Ni-Zn-Sn alloys obtained at a heating rate of 0.167 K/s (0.167 °C/s). The same W/g and temperature scales have been used for representing both DSC plots.

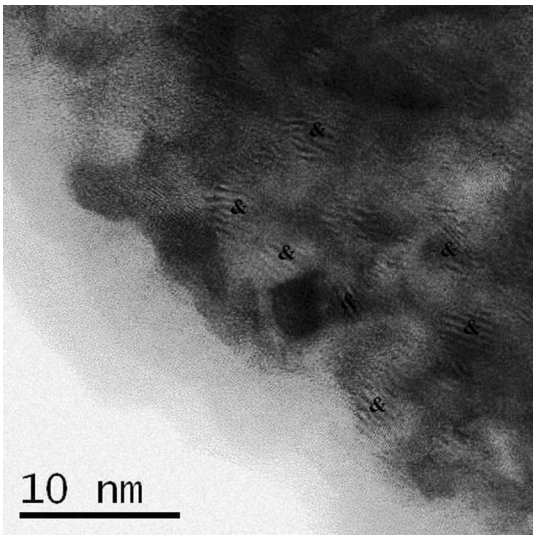

Fig. 2—HRTEM picture of the Cu-Ni-Zn-Sn alloy annealed at 525 K (252 °C) showing Cu2NiZn precipitates.

252 °C), which are in the temperature range of the exothermic DSC peak of the Cu-11Ni-19Zn-1Sn alloy in Figure 1. The maximum value of 186 HV reached by the aging hardening of this alloy is almost twice than the attained by the Cu-11Ni-20Zn alloy, which remarks the noticeable improvement of the mechanical properties of the Cu-Ni-Zn alloy because of the addition of tin. Moreover, the fact that the hardness increases as far as the exothermic peak (Figure 1) is in progress suggests that the improvement of the mechanical properties is due to the Cu_2NiZn nanophase precipitation shown in Figure 2 and allows us to confirm that the annealing temperatures required for the aging hardening of Cu-Ni-Zn-Sn quaternary alloys is considerably lower than those reported for Cu-Ni-Zn-Al alloys.[14] Finally, the data included in Table I point out that the annealing of the alloy at 675 K (402 °C), at which the second endothermic DSC peak in Figure 1 is over, leads to a dramatic decrease of the Vickers hardness until reaching the value reported for the tempered alloy. These results support that the endothermic effect is associated to the solution of the precipitates previously formed for regenerating the starting Cu-11Ni-19Zn-1Sn homogeneous solid solution. Moreover, it is demonstrated that the solvus temperature of this alloy is considerably lower than the one reported[14] for a Cu-Ni-Zn-Al alloy of similar composition in which the tin has been replaced by aluminum.

It has been considered of interest to perform the kinetic analysis of two solid-state reactions, respectively, associated to the exothermic and endothermic DSC peaks of the Cu-11Ni-19Zn-1Sn alloy shown in Figure 1 in order to get a deeper insight in the mechanism of the transitions taking place along the aging treatment of this alloy. The activation energy has been evaluated by the Kissinger method[24] that allows determining this parameter from the temperature corresponding to the maximum rate of the DSC peaks recorded at different heating rates without any previous assumption of the kinetic model fitted by the reaction. It is noteworthy to point out that this method was originally developed for "n order" reactions, but it has been demonstrated that it can be generalized for the whole set of kinetic models proposed in the literature for describing solid-state reactions.[25–28] A set of DSC diagrams of the Cu-11Ni-19Zn-1Sn alloy were obtained at heating rates ranging from 0.083 K/s to 0.667 K/s (0.083 °C/s to 0.667 °C/s) for performing the kinetic analysis by the Kissinger method. The temperatures at the top of the endothermic and exothermic DSC curves, respectively, are plotted as a function of the heating rate in Figure 3.

The Kissinger method is represented by the following equation:

$$\ln \frac{\beta}{T_p^2} = -\frac{E}{RT_p} + \text{Constant}, \qquad [1]$$

where β is the heating rate, T_p is the temperature at the maximum of the DSC peak at a given heating rate, R is the gas constant, and E is the activation energy.

The slope of the plot of the left-hand side of Eq. [1] *vs* the reverse of temperature would lead to the activation energy. The Kissinger activation energies obtained from the exothermic and endothermic DSC peaks, respectively, are included in Table II.

The Kissinger method allows determining the real value of the activation energy but not the kinetic model obeyed by the reaction. The kinetic model could be discerned from the kinetic analysis of a single DSC trace according to the following equation that has been obtained by integrating the Arrhenius equation according with the Doyle approximation[29] that leads to errors in the activation energy lower than 0.02 pct for E/RT values that, like in our case, are higher than 100.[30] The Doyle approximation can be represented by the following equation:

$$\ln g(\alpha) = \ln \frac{AE}{\beta R} - 5.330 - 1.05 \frac{E}{RT}, \qquad [2]$$

where α is the reacted fraction at the temperature T, A is the pre-exponential factor of Arrhenius, and $g(\alpha)$ is a

Table I. Vickers Microhardness as a Function of Time and Annealing Temperature

Alloy	T (K)	t (s)	HV
Cu-Ni-Zn	450 (177 °C)	0	86 ± 2
		7200	95 ± 3
		14,400	102 ± 3
Cu-Ni-Zn-Sn	450 (177 °C)	0	126 ± 3
		5400	146 ± 4
		10,800	164 ± 4
	525 (252 ºC)	0	126 ± 3
		5400	166 ± 4
		10,800	186 ± 5
	675 (402 ºC)	0	126 ± 3
		5400	131 ± 3
		10,800	128 ± 3

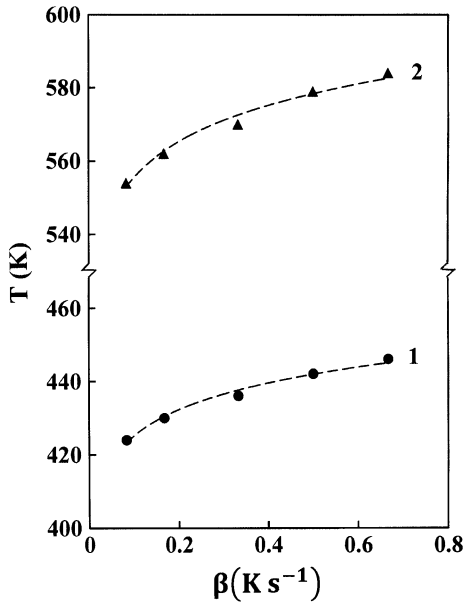

Fig. 3—Peak temperatures of the exothermic (**1**) and the endothermic (**2**) DSC curves of the Cu-Ni-Zn-Sn alloy as a function of the heating rate.

Table II. Kinetic Parameters and Kinetic Functions Obtained from the Kinetic Analysis of DSC Curves

	E (kJ mol^{-1})	$^{*}\ln A$	Kinetic Function
Peak 1	148 ± 2	20.5 ± 0.5	$^{**}[-\ln(1-\alpha)]^{1/n}$
Peak 2	194 ± 3	23.7 ± 0.5	$1-(1-\alpha)^{2/3}$

$^{*}A$ in s^{-1}, $^{**}n = 1.5$.

function depending on the kinetic model obeyed by the reaction.

The activation energy and the pre-exponential factor of Arrhenius would be obtained from the slope and the intercept, respectively, of the plot of the left-hand side of Eq. [2] *vs* the reverse of temperature, provided that the $g(\alpha)$ function really obeyed by the reaction is selected for performing the kinetic analysis. However, we must bear in mind that it has been shown in the literature[28] that a large number of different $g(\alpha)$ functions describing solid-state reactions can fit Eq. [2] leading to strongly different values of the activation energy depending on the kinetic model selected for fitting Eq. [2]. Thus, the kinetic analysis of a single DSC curve does not allow discerning the real kinetic model without additional information. The knowledge of the real value of the activation energy, previously determined from the Kissinger method, would permit to discern the kinetic model of the reaction. This is because only the $g(\alpha)$ function corresponding to the kinetic model really obeyed by the reaction leads to activation energy equal to that determined from the Kissinger method.

The values of the reacted fraction, α, at a given temperature were determined from the ratio between the area enclosed until the corresponding temperature and the total area of the DSC peak. The kinetic analysis of the DSC exothermic peak (peak 1) of the Cu-11Ni-19Zn-1Sn alloy from Eq. [2] is shown in Figure 4. The kinetic function leading to the activation energy in good agreement with the one determined from the Kissinger method has been $g(\alpha) = [-\ln(1-\alpha)]^{1/1.5}$. The value of the pre-exponential factor obtained from the plot of Figure 4 has been included in Table II together with the value of the activation energy. This function is ascribed to phase transitions taking place through an Avrami–Erofeev kinetic model with a coefficient $n = 1.5$. This value of the Avrami–Erofeev coefficient agrees with that to be expected for processes that take place by instantaneous nucleation of nuclei of any shape (needle, plates, spheres) that growth through a diffusion process.[31,32] These results suggest that the precipitates of Cu_2NiZn were generated by the growing of nuclei by a diffusion mechanism. The fact that activation energy reported in Table II is noticeably lower than the diffusion energies of Ni into Cu (204 kJ mol^{-1}), Zn into Cu (185 Kj mol^{-1}) and Sn into Cu (196 kJ mol^{-1})[33] that would be attributed to the extra energy stored by lattice defect generated during the quenching of the alloy. These lattice defects would act as germs for the formation and growth of nuclei. The Avrami–Erofeev kinetic model here found for the precipitation of Cu_2NiZn nanocrystals agrees with the mechanism generally proposed for crystallization and phase transitions in solid state.[31]

The kinetic analysis of the DSC endothermic peak (peak 2 in Figure 1) following the same procedure previously described has led to a kinetic model expressed

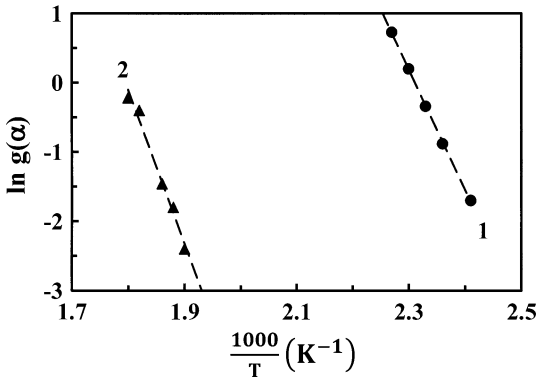

Fig. 4—(**1**) Plot of the values of ln $g(\alpha)$ = ln $[-\ln(1-\alpha)]^{1/1.5}$ calculated from the exothermic DSC curve in Fig. 1 as a function of their corresponding 10^3/T. (**2**) Plot of the values of ln $g(\alpha)$ = ln$[1-(1-\alpha)]^{2/3}$ calculated from the endothermic DSC curve in Fig. 1 as a function of their corresponding 10^3/T.

by the function $g(\alpha) = 1-(1-\alpha)^{2/3}$ as shown in Figure 4. The Arrhenius pre-exponential factor obtained from this plot is included in Table II together with the activation energy that agrees with the corresponding Kissinger activation energy. The fitting of these kinetic models means that the reaction rate is proportional to the surface of the interphase between the spherical particles of the precipitates and the alloy matrix as would be expected for solid-state solution processes.[34] Moreover, the fact that the activation energy shown in Table II for the endothermic peak should roughly agree with the diffusion energies of nickel and zinc into copper suggests that the solution process is controlled by the diffusion of nickel and/or zinc from the surface of Cu_2NiZn precipitates toward the copper matrix. The kinetic analysis supports that the first DSC peak of the Cu-11Ni-19Zn-1Sn alloy is associated to the crystallization of Cu_2NiZn precipitates, while the second one is associated to the solution of these precipitates, as previously concluded from a comparison of DSC peak temperature and HRTEM structural analysis.

IV. CONCLUSIONS

The combined analysis of HRTEM observations, DSC, and microhardness measurements has pointed out that the age hardening of a Cu-11Ni-19Zn-1Sn alloy takes place through a mechanism that implies the precipitation of Cu_2NiZn nanocrystals. The poor hardening response observed by aging a Cu-11Ni-20Zn alloy support that the precipitation of Cu_2NiZn nanocrystals is exclusively induced by the addition of tin to Cu-Ni-Zn alloys leading to a very large improvement of the mechanical properties of the quaternary alloy. The kinetic model proposed from the kinetic analysis of the exothermic DSC peaks of the Cu-11Ni-19Zn-1Sn alloy is in agreement with that to be expected for crystallization of precipitates, while the kinetic law obeyed by the corresponding endothermic peak is that would be expected for the solution of the precipitates previously formed. The comparison of these results with those previously reported by us for a Cu-Ni-Zn alloy of similar composition but with aluminum instead of tin point out that both the annealing temperatures required for age hardening and the solvus temperature of the Cu_2NiZn precipitates into Cu-Ni-Zn-Sn alloys are considerably lower than those found for Cu-Ni-Zn-Al alloys.

ACKNOWLEDGMENTS

The authors would like to acknowledge the Fondo Nacional de Desarrollo Científico y Tecnoloógico (FONDECYT) for financial support, Project No. 1140782. The access to specialized facilities and laboratories provided by the Instituto de Ciencias de Materiales de Sevilla, Spain and the Departamento de Ciencia de los Materiales, Facultad de Ciencias Físicas y Matemáticas, Universidad de Chile is also greatly appreciated.

REFERENCES

1. R.H. Palma, A. Sepúlveda, R. Espinoza, A. Zúñiga, M.J. Diánez, J.M. Criado, and M.J. Sayagués: *Mater. Sci. Eng. A*, 2004, vol. 384, pp. 262–69.
2. J.R. Groza and J.C. Gibeling: *Mater. Sci. Eng. A*, 1993, vol. 171, pp. 115–25.
3. N. Lebrun and P. Perrot: *Non-ferreous metal systems, Part 3, Landolt-Börnstein-Group IV Physical Chemistry*, Springer, Stuggart, 2007, vol. 11C3, pp. 338–54.
4. S. Nagarjuna, M. Srinivas, and K.K. Sharma: *Acta Mater.*, 2000, vol. 48, pp. 1807–13.
5. S. Nagarjuna, B. Gopalakrishna, and M. Srinivas: *Mater. Sci. Eng. A*, 2006, vol. 429, pp. 169–72.
6. X.Z. Zhou, Y.C. Su, and J.M. Sun: *J. Mater. Sci.*, 2010, vol. 45, pp. 3080–87.
7. X.Z. Zhou and Y.C. Su: *Mater. Sci. Eng. A*, 2010, vol. 527, pp. 5153–56.
8. X.P. Ding, H. Cui, J.X. Zhang, H.X. Li, M.X. Guo, and Z.L. Min: *Mater. Des.*, 2015, vol. 65, pp. 1229–35.
9. X.Y. Liu, Q.L. Pan, S.X. Zhang, S.X. Liang, L.Y. Zheng, F. Gao, and H.L. Xie: *Mater. Des.*, 2014, vol. 58, pp. 247–51.
10. C. Li, D.G. Lee, X.J. Mi, W.J. Ye, SX Hui, and YT Lee: *Metall. Mater. Trans. A*, 2016, vol. 47A, pp. 2454–61.
11. G. Miyamoto, S. Suetsugu, K. Shimbo, and T. Furuhara: *Metall. Mater. Trans. A*, 2015, vol. 46A, pp. 5011–20.
12. J.S. Pérez, R.R. Ambriz, F.F.C. López and D.J. Vigueras: *Metall. Mater. Trans. A*, 2016, vol. 47A, pp. 3412–22.
13. S. Sackl, M. Zuber, H. Clemens, and S. Priming: *Metall. Mater. Trans. A*, 2016, vol. 47A, pp. 3694–3702.
14. M.J. Diánez, E. Donoso, J.M. Criado, M.J. Sayagués, G. Diaz, and L. Olivares: *Mater. Des.*, 2016, vol. 92, pp. 184–88.
15. T.D. Shen and C.C. Koch: *Acta. Mater.*, 1996, vol. 44, pp. 753–61.
16. E. Donoso, R. Espinoza, M.J. Diánez and J.M. Criado: *Mater. Sci. Eng. A*, 2012, vol. 556A, pp. 612–16.
17. S. Sheibani, S. Heshmati-Manesh, A. Ataie, A. Caballero, and J.M. Criado: *J. Alloys Compd.*, 2014, vol. 587, pp. 670–76.
18. T. Klassen, U. Herr, and R.S. Averback: *Acta Mater.*, 1997, vol. 45, pp. 2921–30.
19. S. Sheibani, A. Ataie, S. Heshmati-Manesh, A. Caballero, and J.M. Criado: *Thermochim. Acta*, 2011, vol. 526, pp. 222–28.
20. M.J. Diánez, E. Donoso, M.J. Sayagués, A. Perejón P.E. Sánchez-Jiménez, L.A. Pérez-Maqueda, and J.M. Criado: *J. Alloys Compd.*, 2016, vol. 688, pp. 238–94.
21. E. Donoso, A. Zúñiga, M.J. Diánez, and J.M. Criado: *J. Thermal Anal. Calorim.*, 2010, vol. 100, pp. 975–80.
22. E. Donoso, G. Díaz, and J.M. Criado: *J. Thermal Anal. Calorim.*, 2008, vol. 91, pp. 491–95.

23. S. Esmaeili, X. Wang, D.j. Lloyd and W.J. Poole: *Metall. Mater. Trans. A*, 2003, vol. 34A, pp. 751–63.
24. H.E. Kissinger: *Anal. Chem.*, 1957, vol. 29, pp. 1702–06.
25. J.M. Criado and A. Ortega: *J. Non-Cryst. Solids*, 1986, vol. 87, pp. 302–11.
26. J.M. Criado and A. Ortega: *Acta Metall.*, 1987, vol. 35, pp. 1715–21.
27. D. Chen, X. Gao, and D. Dollimore: *Thermochim. Acta*, 1993, vol. 215, pp. 109–17.
28. S. Vyazovkin, A.K. Burhan, J.M. Criado, L.A, Pérez-Maqueda, C. Popescu, and N. Sbirrazzuoli: *Thermochim. Acta*, 2011, vol. 520, pp. 1–19.
29. C.D. Doyle: *Nature*, 1966, vol. 20, p. 290.
30. L.A. Pérez-Maqueda, P.E. Sánchez-Jiménez, and J.M. Criado: *Int. J. Chem. Kinet.*, 2005, vol. 37, pp. 658–66.
31. J.W. Christian: *The Theory of Transformations in Metals and Alloys*, 3rd ed., Pergamon Press, London, U.K., 2002, pp. 529–52.
32. Z. Chvoj, J. Sestak, and A. Tritska: *Kinetic Phase Diagrams. Non-equilibrium Phase Transitions*, Elsevier, Amsterdam, The Netherland, 1991, p. 222.
33. A.M. Brown and M.F. Ashby: *Acta Metall.*, 1980, vol. 28, pp. 1266–71.
34. A. Varchavsky and E. Donoso: *J. Miner. Met.*, 1999, vol. 35B, pp. 255–76.